

# Efficiency and Forward Voltage of Blue and Green Lateral LEDs with V-shape defects and Random Alloy Fluctuation in Quantum Wells

Cheng-Han Ho,<sup>1</sup> James S. Speck,<sup>2</sup> Claude Weisbuch,<sup>2,3</sup> and Yuh-Renn Wu<sup>1,4, a)</sup>

<sup>1)</sup>*Graduate Institute of Photonics and Optoelectronics, National Taiwan University, Taipei 10617, Taiwan*

<sup>2)</sup>*Materials Department, University of California, Santa Barbara, California 93106, USA*

<sup>3)</sup>*Laboratoire de Physique de la Matière Condensée, Ecole Polytechnique, CNRS, IP Paris, 91128 Palaiseau Cedex, France*

<sup>4)</sup>*Electronic and Optoelectronic System Research Laboratories, Industrial Technology Research Laboratories, Hsinchu, Taiwan.*

(Dated: 11 February 2022)

For nitride-based blue and green light-emitting diodes (LEDs), the forward voltage  $V_{\text{for}}$  is larger than expected, especially for green LEDs. This is mainly due to the large barriers to vertical carrier transport caused by the total polarization discontinuity at multiple quantum well and quantum barrier interfaces. The natural random alloy fluctuation in QWs has proven to be an important factor reducing  $V_{\text{for}}$ . However, this does not suffice in the case of green LEDs because of their larger polarization-induced barrier. V-defects have been proposed as another key factor in reducing  $V_{\text{for}}$  to allow laterally injection into multiple quantum wells (MQWs), thus bypassing the multiple energy barriers incurred by vertical transport. In this paper, to model carrier transport in the whole LED, we consider both random-alloy and V-defect effects. A fully two-dimensional drift-diffusion charge-control solver is used to model both effects. The results indicate that the turn-on voltages for blue and green LEDs are both affected by random alloy fluctuations and V-defect density. For green LEDs,  $V_{\text{for}}$  decreases more due to V-defects, where the smaller polarization barrier at the V-defect sidewall is the major path for lateral carrier injection. Finally, we discuss how V-defect density and size affects the results.

## I. INTRODUCTION

Blue nitride-based light-emitting diodes (LEDs) with phosphor have become the major white-light source. However, high-efficiency or micro-LED display applications require green- and red-light sources and, for ultimate efficiency, white-light lamps based on RGB color mixing. Currently, the peak internal quantum efficiency (IQE) of blue LEDs is over 90% at a current density of 1–10 A/cm<sup>2</sup>.<sup>1</sup> However, the IQE of green LEDs remains low, which is likely due to the strong quantum-confined Stark effect induced by the polarization charge and the large defect density<sup>1–3</sup>. In addition, the forward voltage  $V_{\text{for}}$  of green LEDs also exceeds the expected 2.3 V,<sup>4</sup> which also limits the wall plug efficiency.

III-nitrides in the common (0001) orientation have polarization-induced barriers at the InGaN/GaN quantum well/quantum barrier (QW/QB) interface due to spontaneous and piezoelectric polarization differences between the well and barrier materials.<sup>5</sup> The polarization discontinuity at the QW/QB interface results in significant electric fields in the QWs and QBs—often referred to as “piezofields.” For green LEDs, the polarization discontinuity at the QW/QB interface increases due to the increased lattice mismatch between the InGaN and GaN layers.

The influence of polarization-induced barriers has been discussed in many studies<sup>4,6,7</sup> where carriers are easily blocked by the extra potential barrier. Our previous studies of blue LEDs<sup>8,9</sup> show that fluctuations in indium composition provide extra paths for carrier injection. Including random indium composition fluctuations in models thus helps to explain

the lower  $V_{\text{for}}$  in blue LEDs compared with models without fluctuations.<sup>10,11</sup>

To further reduce  $V_{\text{for}}$  in situations with larger barriers, such as in green LEDs, it is important to either reduce the polarization field or find an alternative way to inject carriers. The most significant method is by controlling the V-shaped defect (V-defect) opened at the InGaN/GaN MQW active regions to provide an alternative way to inject carriers. Most V-defects are the result of dislocation lines that form under certain growth conditions.<sup>12–14</sup> Unlike the threading dislocation (TD) centers, which are typical nonradiative centers, the inclined sidewalls of V-defects reportedly assist carrier injection into QWs.<sup>15–17</sup> Since both random alloy fluctuations and V-defects provide concurrent paths for carrier injection, it is important to model both effects in carrier injection simultaneously. The importance of considering both mechanisms is obvious as the paper leads to the conclusion that random alloy fluctuations suffice to lead to efficient low-voltage injection in blue LEDs while V-defects are needed to achieve this in longer wavelength LEDs in the green spectral range.

Given that V-defects play an important role in carrier injection, it is important to understand the role of random alloy fluctuations and of V-defects in carrier injection. The V-defect and random alloy effects may be simulated separately in three-dimensional simulations.<sup>8,15</sup> On the one hand, V-defects range from a few hundred nanometers in size to the  $\mu\text{m}$  scale, allowing for large mesh sizes. On the other hand, random alloy fluctuations occur on a scale of a few nanometers, requiring mesh elements to be as small as possible to account for such small-scale fluctuations. Including both effects in a three-dimensional simulation requires unreasonable computer memory (> a few TB) and computing times. However, to understand the influence of random alloy fluctuation

<sup>a)</sup> Author to whom correspondence should be addressed: yrwu@ntu.edu.tw

and V-defect on the efficiency of LEDs, especially for green LEDs, it is essential to include both effects simultaneously. Recent results on the lateral carrier diffusion<sup>18</sup> in QW show that the random alloy fluctuations strongly limits carrier diffusion. Hence, if the carriers are only injected through V-defects, the current spreading to the whole QW area from the V-defect will be limited, which is observed without considering random alloy fluctuation. Furthermore, the improvement in turn-on voltage induced by V-defects, critical to the wallplug efficiency, can be jeopardized by the adverse action of the threading dislocation within the V-defects as nonradiative centers on the *IQE*. The balance between the reduction of  $V_{\text{for}}$  by increasing the V-defect density and the simultaneous decrease in *IQE* must be explored. A compromise to the present difficulties of 3D simulations is to work on two-dimensional (2D) simulations that include random alloy fluctuations and V-defects. Some issues might be missed in the 2D model, such as the estimation of carrier quantum confinement effects occurring in 3D. This may affect the estimation of carrier overlap in random alloy fluctuating potentials. The V-defect filling factor of 2D and 3D models may not be equal and needs some translation. However, the 2D model enables us to calculate the whole LED structure, including the current crowding effect. This helps us to understand the simultaneous influences of V-defect density and random alloy fluctuation to  $V_{\text{for}}$  or and *IQE*. In this paper, we discuss the influence of V-defects and random alloy fluctuations with such an alternative 2D model.

V-defects may be controlled by tuning the growth conditions. Often, V-defects are formed in the widely used InGaN/GaN short periodic superlattice that is grown before growing active InGaN/GaN QWs.<sup>19</sup> The general V-defect density is about  $1 \times 10^7 \text{ cm}^{-2} \sim 5 \times 10^8 \text{ cm}^{-2}$ , and the typical diameter is about 30–250 nm for five QWs in blue LEDs.<sup>12–14,19</sup> Hence, in this paper, we will cover the V-defect density from 0 to  $\sim 6.25 \times 10^8 \text{ cm}^{-2}$ . Furthermore, V-defects form an inverted hexagonal pyramid with six inclined  $\{10\bar{1}1\}$  semipolar sidewalls.<sup>20</sup> Studies show that the indium composition in *c*-plane QWs is greater than in the inclined QWs in the V-defect region.<sup>21</sup> Therefore, the bandgap of QWs in the inclined sidewall of V-defects is larger than the bandgap of QWs in the *c* plane. The polarization discontinuity between the semipolar  $\{10\bar{1}1\}$  InGaN sidewall QW and QB is much smaller than the *c*-plane QW and is in the opposite direction.<sup>22</sup> Thus, holes can be injected into the QWs in the *c* plane through the sidewall V-defect QWs with lower barrier potentials.<sup>23</sup> The additional paths provided decreased  $V_{\text{for}}$  and increase the carrier-injection efficiency.<sup>24–26</sup> However, V-defects form at TDs, and a high density of nonradiative centers at the center of V-defects could be a drawback. Thus, the density and diameter of the V-defects in the LED should be optimized to minimize this counter-acting effect.<sup>27</sup>

In this paper, we use simulations to investigate how random fluctuations and V-defects affect InGaN-based LEDs. As mentioned above, computer-memory limitations oblige us to use 2D simulations with fluctuations instead of three-dimensional simulations. In 2D simulations, the size of the simulated structure may be increased to the micron scale to

approach the real device structure of LEDs. In the following, we discuss the 2D structure with different V-defect densities and diameters (lateral size). The forward voltage  $V_{\text{for}}$  and efficiencies (electrical and *IQE*) are discussed and explained by the interplay between lateral carrier injection through the V-defect sidewalls and subsequent carrier diffusion within the planar QW regions.

## II. METHODOLOGY

To simulate random alloy fluctuations in devices, we use an in-house-developed 2D drift-diffusion charge control solver to determine the electrical carrier distribution, recombination rates, and other properties. First, to account for the random alloy fluctuations and V defects, we construct a mesh for a device with a V-defect. The mesh size at the QW region is 0.5 nm in the *x* direction and 0.1 nm in the *z* direction. The mesh size is larger in the *p* and *n* layers to save computer memory. We then use a random number generator to create the random atom distribution in the alloy regions<sup>28</sup> and subsequently use Gaussian averaging to assign the local indium composition in the QWs.<sup>29–31</sup>

Figure 1 shows the indium composition fluctuations in the QWs, where the bandgap depends on the indium composition. Note that, in the 2D simulation, we cannot calculate the real strain distribution with a strain solver because we have neglected the third dimension. Thus, fully compressive strain is assumed when calculating the lattice size of the GaN buffer layer based on the local indium composition. We then calculate the local material parameters such as bandgap, conduction- and valence-band energies, polarization according to the local indium composition, and strain state. In addition, we use the localization landscape (LL) model<sup>29,32,33</sup> shown in Eq. (2) instead of the Schrödinger equation solver to obtain the effective quantum potential seen by the carriers.<sup>31</sup>

### A. Methodology of analyzing two-dimensional solver

To simulate the 2D Poisson, drift-diffusion, and LL equations, the following equations were used:

$$\nabla \cdot (\epsilon \nabla \phi) = q(n - p + N_A^- - N_D^+ \pm \rho_{\text{pol}}), \quad (1)$$

$$\left[ -\frac{\hbar^2}{2} \nabla \cdot \left( \frac{1}{m_{e,h}^*} \nabla \right) + E_{c,v} \right] u_{e,h} = 1, \quad (2)$$

$$n = \int_{1/u_e}^{+\infty} \text{LDOS}(E) \frac{1}{1 + \exp\left(\frac{E - E_{Fn}}{k_B T}\right)} dE, \quad (3)$$

$$p = \int_{1/u_h}^{-\infty} \text{LDOS}(E) \frac{1}{1 + \exp\left(\frac{E_{Fp} - E}{k_B T}\right)} dE, \quad (4)$$

$$J_{n,p} = \mu_{n,p}(n, p) \nabla E_{F_{n,p}}, \quad (5)$$

$$\frac{1}{q} \nabla \cdot (J_{n,p}) = R_{n,p} - G_{n,p}, \quad (6)$$

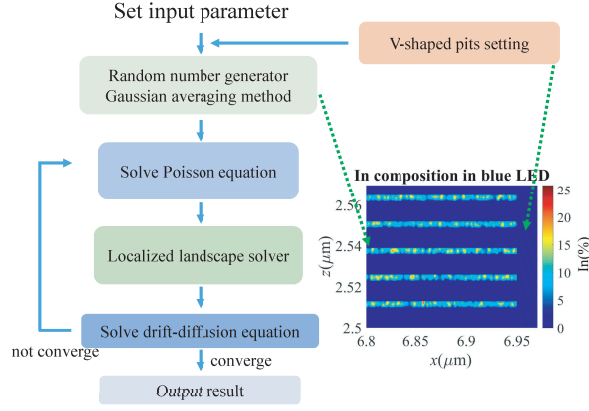


FIG. 1. Flow chart of simulation model. The mesh with V-defect shapes is put in the simulation program. The random alloy map is generated by using a random number generator and then put in the solver to realize convergence after the required number of feedback loops. The right panel shows the indium composition map in the MQWs.

$$R = R_{\text{SRH}} + B_0 np + C_0 (n^2 p + np^2), \quad (7)$$

$$R_{\text{SRH}} = \frac{np - n_i^2}{\tau_{n0}(p + n_i) + \tau_{p0}(n + n_i)}. \quad (8)$$

In these equations,  $\phi$  is the electrostatic potential in the structure,  $n$  and  $p$  are the free electron and hole concentrations, and  $N_A^-$  and  $N_D^+$  are the ionized acceptor and donor concentrations determined by the ionization energy (and position in the junction and junction electric field), respectively.  $\rho_{\text{pol}}$  is the polarization charge that has been computed from the divergence of the total polarization, and  $\frac{1}{u_e}$  and  $\frac{1}{u_h}$  are the effective quantum potentials of electrons and holes calculated by the LL equations,<sup>29,33</sup> respectively.

First, we calculate  $\phi$  by using the Poisson equation (1) and obtain the local band extrema  $E_c$  and  $E_v$  through the local  $\phi$  and alloy composition. Then, the LL equations (2) are solved to yield  $u_e$  and  $u_h$  and the effective quantum potentials  $\frac{1}{u_e}$  and  $\frac{1}{u_h}$ . The carrier distributions are calculated by using Eqs. (3) and (4), the effective quantum potentials  $\frac{1}{u_e}$  and  $\frac{1}{u_h}$ , and the quasi-Fermi levels  $E_{Fn}$  and  $E_{Fp}$ . Finally, we determine  $E_{Fn}$  and  $E_{Fp}$  from Eqs. (5) and (6). The recombination rate is given by Eq. (7), and includes radiative recombination ( $IQE$ ), Auger recombination, and Shockley–Read–Hall (SRH) recombination.  $B_0$  is the radiative recombination rate. Equation (8) is the SRH recombination equation, where  $\tau_n$  and  $\tau_p$  are the nonradiative carrier lifetimes of electrons and holes, respectively.  $C_0$  is the Auger recombination rate coefficient, which is the recombination of three particles, either directly or mediated by phonons.<sup>34</sup>

Next, we construct the mesh according to the position in the structure; each mesh point has different parameters. To simulate V-defects in the structure, the mesh is readjusted according to the V-defect diameter and density. Finally, these equations are solved self-consistently. Figure 1 shows a de-

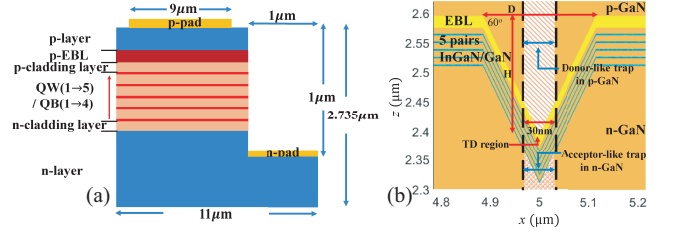


FIG. 2. (a) Simulated structure of lateral LED. (b) Definition of parameters for V-defect structure.

tailed flowchart of the simulation.

## B. Device structures and parameters

To discuss the V-defect, we analyze the blue and green LEDs with the structure shown in Fig. 2(a). The chip lateral size is  $11 \mu\text{m}$  and the region of multiple quantum wells (MQWs) is  $10 \mu\text{m}$  wide, which is also defined as the total region. Since our mesh element size is quite small compared to the size of the device, we use about  $1.1 \times 10^7$  nodes to simulate the  $11 \mu\text{m}$  chip, which requires 55 GB of memory to run the 2D simulation. The  $p$  contact (in common  $p$ -side LEDs, this layer is made from indium tin oxide) is about  $9 \mu\text{m}$  wide at the center of the active region, and the  $n$  pad is about  $1 \mu\text{m}$  wide.

For the blue and green LEDs, we consider a MQW LED with a  $0.14 \mu\text{m}$  top  $p$ -GaN layer doped at  $3 \times 10^{19} \text{cm}^{-3}$ , a  $p$ -AlGaIn electron blocking layer (EBL) and  $p$ -GaInN cladding layer both doped at  $2 \times 10^{19} \text{cm}^{-3}$ , five QWs and four QBs between the QWs are unintentionally doped  $n$  type at  $1 \times 10^{17} \text{cm}^{-3}$ , one  $10 \text{nm}$   $n$ -cladding layer and then a  $2.5 \mu\text{m}$   $n$ -GaInN layer doped at  $5 \times 10^{18} \text{cm}^{-3}$ . The doping density of the  $n$ -type cladding layer is  $1.0 \times 10^{19} \text{cm}^{-3}$ . For the green LED, the first two QBs are  $n$  doped at  $1.0 \times 10^{18} \text{cm}^{-3}$  to partially screen the piezoelectric field for better vertical carrier injection. We also ran a simulated case without doping in the first two QBs (and with no V-defects) for comparison. In addition,  $\tau_n$  and  $\tau_p$  for the blue and green LEDs are 100 and 10 ns, respectively, because the green LED has a higher In content in the InGaInN than the blue LED and thus a lower growth temperature, which leads to a higher density of SRH centers in the real device. The detailed parameters of the structures are shown in Table I. For the blue LED, the average indium composition in the QWs is 13% ( $\text{In}_{0.13}\text{Ga}_{0.87}\text{N}$ ). For the green LED, the average indium composition in the QWs is 22% ( $\text{In}_{0.22}\text{Ga}_{0.78}\text{N}$ ). Additionally, alloy fluctuations in the InGaInN layers are included in both the blue and green LEDs. The  $B_0$  is  $2 \times 10^{-11} \text{cm}^3/\text{Vs}$  and the  $C_0$  is  $2 \times 10^{-31} \text{cm}^6/\text{Vs}$ . These two parameters are not changed in the simulation since we focus on V-defect and random alloy fluctuation influences. The influence of overlap due to the different QCSE and disorder is included in the term of  $n(r) \times p(r)$ .

Figure 2(b) shows the geometrical definition of V-defects, where  $H$  and  $D$  are the depth and diameter of the V-defect, respectively. We use these parameters in the following discus-

TABLE I. Basic parameters of blue and green LEDs.

Area	Material unit	Thickness nm	Doping blue , green $10^{18}\text{cm}^{-3}$	$E_a$ meV	e, h mobility $\text{cm}^2/\text{V s}$	$\tau_n, \tau_p$ blue ns	$\tau_n, \tau_p$ green ns
<i>p</i> layer	<i>p</i> -GaN	140	30, 30	180	100, 5	100	10
<i>p</i> EBL	<i>p</i> -AlGaIn	20	20, 20	264	100, 5	100	10
<i>p</i> cladding layer	<i>p</i> -GaN	10	20, 20	180	100, 5	100	10
QW(3,4,5)	<i>n</i> -InGaIn	3	0.1, 0.1	25	150, 10	100	10
QB(3,4)	<i>n</i> -GaIn	10	0.1, 0.1	25	350, 10	100	10
QW(1,2)	<i>n</i> -InGaIn	3	0.1, 0.1	25	150, 10	100	10
QB(1,2)	<i>n</i> -GaIn	10	0.1, 1	25	350, 10	100	10
<i>n</i> cladding layer	<i>n</i> -GaIn	10	10, 10	25	200, 10	100	10
<i>n</i> layer	<i>n</i> -GaIn	2500	5, 5	25	200, 10	100	10

TABLE II. Trap parameters in the threading dislocation (TD) center.

Type		
Donor-like	Trap density ( $1/\text{cm}^3$ )	$1 \times 10^{18}$
	Trap $\tau_n, \tau_p$ (ns)	1.01
	$E_t$ below $E_c$ (eV)	1.14
Acceptor-like	Trap density ( $1/\text{cm}^3$ )	$1 \times 10^{18}$
	Trap $\tau_n, \tau_p$ (ns)	0.38
	$E_t$ below $E_c$ (eV)	2.5

sion. The region between the vertical black dotted lines correspond to the TD along the direction  $\{0001\}$  with a 30 nm width at the center of the V-defect, and the V-defect sidewall QWs are inclined about  $60^\circ$  according to both transmission electron microscopy (TEM) and scanning TEM,<sup>35,36</sup> which is consistent with early work showing that the sidewalls are  $\{10\bar{1}1\}$  planes. In addition, the thickness of the *c*-plane QWs is 3 nm. The inclined sidewall QW is also 3 nm thick in the *z* direction, which corresponds to a thickness of 1.73 nm ( $3 \text{ nm} \times \cos 60^\circ$ ) along the normal to the inclined plane.<sup>37</sup> The indium composition in the inclined QWs depends on the composition in *c*-plane QWs. For example, for blue LEDs, the indium composition of inclined QWs is 8%.<sup>38,39</sup> For green LEDs, the indium composition in the inclined QWs is about 16%.<sup>40</sup> In addition, the TDs are defects induced by the lattice and chemical mismatch between the sapphire substrate and GaN.<sup>41,42</sup> Thus, we include TD-associated trap states in the TDs regions, which trap either electron or holes and are shown as the cross-hatched areas in Fig. 2(b). The density of TD-associated trap states is about  $1 \times 10^{18} \text{ cm}^{-3}$  corresponding to one trap state per *c* translation along the dislocation line within the 30 nm diameter TD ranges.<sup>43,44</sup> The trap energy level ( $E_t$ ) is 1.14 eV below  $E_c$  for donor-like traps and 2.5 eV below  $E_c$  for acceptor-like traps, as shown in Table II. The trap lifetimes are also given in Table II.<sup>44</sup>

### III. RESULTS AND DISCUSSION

#### A. Influence of random alloy fluctuations, V-defects, and threading dislocations for the current path

Figure 3 shows the calculated  $E_c$  and effective quantum potential  $\frac{1}{u_c}$  for the blue and green LEDs, taking into account random alloy fluctuations at a bias voltage  $V = 3 \text{ V}$ . A cross section with minimum potential barrier was chosen for the full curves. They show the best case for carrier transport across the QWs. The dashed curves for disorder averaged levels show slightly larger barriers. Without considering the random alloy fluctuation, the voltage voltage would be even higher which has been discussed in ref.<sup>6,8,31</sup>. Hence we will not discuss the cases with and without random alloy fluctuation. Although Figs. 3(a) and 3(b) show that random alloy fluctuations already change the depth of the QWs for blue LEDs (compare the  $E_c$  curves with and without fluctuations), the potential barrier induced by piezoelectric field between QWs is still about 0.4 eV for the blue LED, whose carriers can overcome the barrier through thermal excitation. However, for the green LED, the potential barrier is about 0.7 eV, which strongly impedes carrier transport across the MQWs at the bias  $V = 3 \text{ V}$ . While the current density at that bias is a few  $\text{A}/\text{cm}^2$  for the blue LED [see Fig. 6(a)], it is negligible in the green LED [Fig. 9(a)]. Thus, even when considering random alloy fluctuations, carriers are hardly injected directly into the *c*-plane QW for the green LED, despite the large 0.7 V excess voltage. We also observe that the inclusion of the quantum disorder correction through the use of the LL theory (thus yielding the effective potential  $\frac{1}{u_c}$ ) only weakly diminishes the potential barriers, in particular for the green LED. Reducing  $V_{\text{for}}$  in these LEDs requires the use of another injection mechanism, namely, injection through V-defects.

We first focus on hole injection through a V-defect. Figures 4(a) and 4(b) show the valence-band potential of blue and green LEDs in a V-defect, respectively. First, in the middle of the V-defect, within  $\pm 15 \text{ nm}$  of the TD in the *p*-GaIn layer region, holes are trapped in the hole traps associated with the TD, which repels holes from the TD center [the repelling potential is shown in a lighter color in the TD region in Figs. 4(a) and 4(b)]. Next, holes transport toward the *c*-

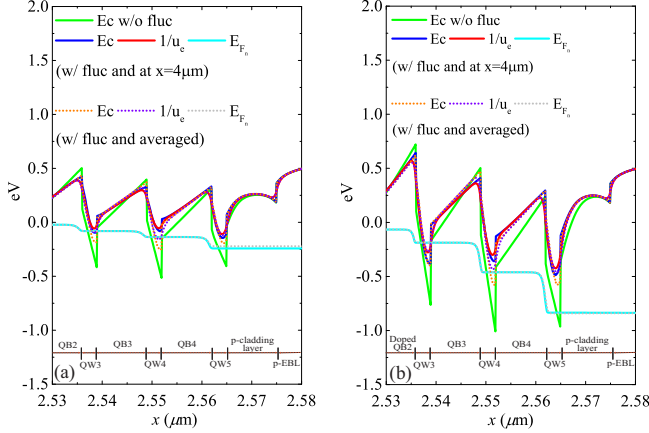


FIG. 3. Cross section plot for the three top QWs of  $E_c$  without fluctuations ( $E_c$  w/o fluc),  $E_c$  with fluctuations ( $E_c$  w/ fluc), effective potential  $\frac{1}{u_c}$ ,  $E_{Fn}$  along  $z$ -direction with random alloy fluctuations but without V-defects. (a) is for the blue LED, and (b) is for the green LED. The applied bias is 3V. The full curves w/ fluc are for the cross section with minimum barrier and the dashed lines are for the fluctuation-averaged potential  $E_c$ ,  $\frac{1}{u_c}$  and  $E_{Fn}$ .

plane QWs through the inclined plane, as shown in Figs. 5(c) and 5(d). Given the position of the electron-injecting region relative to the  $c$ -plane QWs, electrons are first injected into the side-wall QWs, from which they diffuse toward the lower-energy  $c$ -plane QWs.

Figures 4(c) and 4(d) show the radiative recombination map for the blue and green LEDs at  $20 \text{ A/cm}^2$ , respectively. For blue LEDs, recombination occurs throughout the structure as electrons and holes (at least four of the  $c$ -plane QWs for holes) are injected vertically [Figs. 5(a) and 5(c)] in the  $c$ -plane QWs. For the green LED, while electrons are injected both vertically and through the V-defect [Fig. 5(b)], holes are not injected vertically because of the much larger polarization-induced barrier in the  $c$  plane, Holes are therefore injected through the V-defect sidewall near which recombination occurs and decays laterally within a characteristic diffusion length. In addition, only two to three  $c$ -plane QWs receive holes through the V-defect. Both effects limit the effectiveness of V-defects as a solution to excite the whole volume of the  $c$ -plane QWs. For the blue LED, the crowding effect of carriers near V-defects is weaker because holes can still be injected vertically into the whole  $c$ -plane area due to random alloy fluctuations. The relative importance of vertical injection versus V-defect injection is discussed in more detail below along with how the V-defect size and density affects  $V_{\text{for}}$  and the  $IQE$  for blue and green LEDs.

A remarkable phenomenon is seen in Fig. 5: both electrons and holes are preferentially injected into QWs near the middle of the MQW stack, QWS #2, 3, 4 for the blue LED, and QW #4 for the green LED. This is dominantly due to the peculiarity of hole injection through V-defects. Due to the diminished piezo-

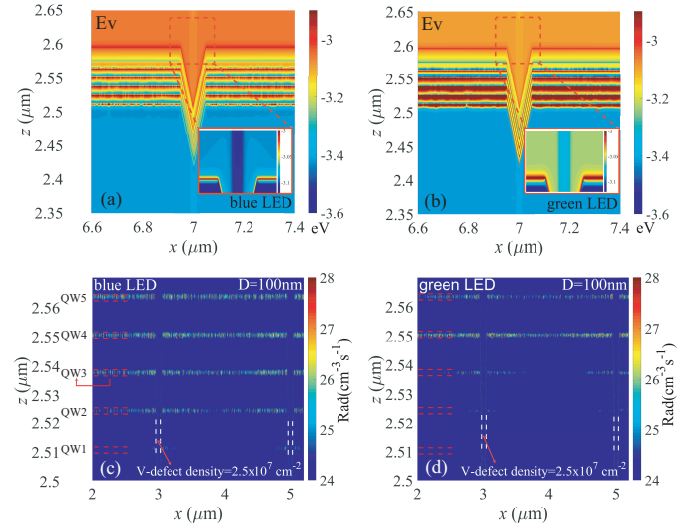


FIG. 4. Valence-band energy and radiative recombination for blue LED and green LED at V-defect density  $2.5 \times 10^7 \text{ cm}^{-2}$  and  $D = 100 \text{ nm}$  at a current density of  $20 \text{ A/cm}^2$ . (a) Valence band for the blue LED, (b) valence band for the green LED, (c) radiative recombination for the blue LED at  $20 \text{ A/cm}^2$ , and (d) radiative recombination for the green LED at  $20 \text{ A/cm}^2$ . The plot is at log scale. White dashed lines show the location of V-defects on the  $x$  axis. Insets in panels (a) and (b) at different color scale emphasize the higher potential energy for holes at the center due to trap charging. The scale color bar ranges from  $-3.0 \text{ eV}$  (red) to  $-3.1 \text{ eV}$  (blue)

electric induced barrier at the sidewall (which is a semipolar plane at 60 degree), the electrons and holes are more easily injected sideways than vertically, especially for holes, which have a heavier effective mass and lower mobility. Due to the  $p$ -doping of the last barrier, holes are easily injected in QW5 through the sidewall. Overcoming one more barrier is still relatively easy for holes, compared to the  $c$ -plane vertical injection. Holes then first meet electrons in QW4 and recombine there. Why aren't electrons injected in QW5? Close inspection of electron current in Fig. 5 (b) for green LEDs show that they experience a significant energy barrier between the side-wall QWs 4 and 5 (blue color of the barrier). This is due to the nearby  $p$  doping inside the V-defect which raises the barrier. The behavior is more significant for the green case as can be seen in Figs. 5(b) and (d), as well as on the recombination current in Fig. 4(d). This was not observed without V-defect since it is much harder for holes to overcome the large piezoelectric barrier in the  $c$ -plane direction especially in the green case. Then, holes are preferentially injected in QW # 5 where they meet electrons. It is well known that holes in the planar LED case are mainly injected in the QW nearest to the  $p$ -side in planar MQW LEDs, and this is of course well reproduced in our other simulation papers which include disorder effects without V-defects.

Since carriers are mainly going through V-defects for the green LED, the density of V-defects play an important role in the LED current-voltage characteristics. Using a high V-defect density to obtain more injection sites, the active  $c$ -plane QW area becomes smaller and the carrier density in the  $c$

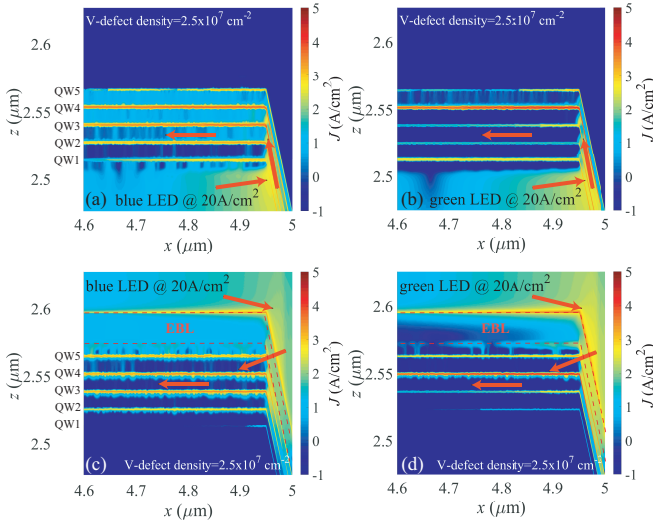


FIG. 5. Current distribution for blue LED and green LED at V-defect density of  $2.5 \times 10^7 \text{ cm}^{-2}$  and  $D = 100 \text{ nm}$  at a current density of  $20 \text{ A/cm}^2$ . (a) Electron current density  $|J_n|$  for blue LED, (b) electron current density  $|J_n|$  for green LED, (c) hole current density  $|J_p|$  for blue LED, and (d) hole current density  $|J_p|$  for green LEDs. The plot is at log scale. The vector sense for the electrons [panels (a) and (b)] and hole [panels (c) and (d)] are shown by the red arrows.

plane increases for the same current. This adversely affects the  $IQE$  and droop behavior.<sup>45</sup> Therefore, it is important to discuss in detail how the V-defect density and size affect the LED structure.

## B. Influence of V-defects and random alloy fluctuations on $I$ - $V$ and $IQE$

The influence of V-defects for the specific lateral LED of Fig. 2 is now discussed for green and blue LEDs. The effects on  $IQE$  and  $V_{\text{for}}$  of both random alloy fluctuations and V-defects are simulated for different V-defect densities and diameters. We use V-defect densities of  $1 \times 10^6$ ,  $2.5 \times 10^7$ ,  $1 \times 10^8$ ,  $2.25 \times 10^8$ , and  $6.25 \times 10^8 \text{ cm}^{-2}$  and V-defect diameters of 50, 100, 220, 280, and 340 nm.

### 1. Performance of blue V-defect LED

We first discuss the dependence of  $V_{\text{for}}$  on the V-defect density. Here we define the forward voltage  $V_{\text{for}}$  as the voltage needed for a current density of  $1 \text{ A/cm}^2$ . Figure 6(a) shows the results for the blue LED structures without and with the V-defects. The V-defect diameter is 100 nm.  $V_{\text{for}}$  is about 2.88 V for the case without V-defects. The maximum density of V-defects is  $6.25 \times 10^8 \text{ cm}^{-2}$ , and  $V_{\text{for}}$  for this case is about 2.74 V at  $1 \text{ A/cm}^2$ , which equates to about zero excess voltage.

For a V-defect density of  $1 \times 10^8 \text{ cm}^{-2}$ , Fig. 6(b) shows the dependence on V-defect size. The results show that the

voltage decreases as the V-defect diameter increases from 50 to 100 nm, but  $V_{\text{for}}$  remains constant for the larger V-defect diameters, with all the decrease in  $V_{\text{for}}$  already realized at the lateral V-defect size of 50 nm. One factor contributing to this result is that the voltage is already close to  $\frac{h\nu}{e}$ , leaving little possibility for further reduction of  $V_{\text{for}}$ .

Figure 6(c) shows the  $IQE$  of blue LEDs with different V-defect densities; the  $IQE$  peak slightly decreases as the V-defect density increases. For high V-defect densities, the  $IQE$  peak appears at higher current density. In the low-current-density region ( $10^{-3}$  to  $1.0 \text{ A/cm}^2$ ), holes are injected mainly through V-defects and electrons are injected vertically through the random alloy fluctuating potential, whereas for higher current density, the higher  $V_{\text{for}}$  means that both carriers start to be injected directly from the  $c$ -plane QW through the fluctuating potential barriers. Since the V-defect center contains strong nonradiative recombination (NR) centers, carriers are injected through V-defects experience more NR.

Figures 7(a) and 7(b) show the radiative recombination for current densities of  $10^{-2}$  and  $20 \text{ A/cm}^2$ , respectively, for blue LEDs at a V-defect density of  $2.5 \times 10^7 \text{ cm}^{-2}$ . At low current density, the top QW shows weak radiative recombination, which means that holes are injected from V-defects due to the diminished piezoelectric field-induced barrier at the sidewall, especially for holes with lower mobility. At high current density, the top QW also emits light because holes are also injected vertically. Thus, at higher current density, the  $IQE$  and  $V_{\text{for}}$  are less influenced by V-defects and the dislocation region. More QWs emit light, and the impact of NR diminishes, so all curves regroup.

Figures 7(b)–7(d) show the recombination distribution for different V-defect densities at  $J = 20 \text{ A/cm}^2$ . The crowding effect is limited because of vertical injection through random alloy fluctuations but is significant at low V-defect density. Note that if random alloy fluctuations are not considered in the  $c$ -plane QW, carrier diffusion extends much further. Then, we do not observe current crowding near V-defect for the lower V-defect density, making the predicted  $IQE$  higher. Increasing the V-defect density diminished the crowding effect and thus moves the peak  $IQE$  to a higher current density, although the peak  $IQE$  is diminished somewhat because of the increased density of NR centers [Fig. 6(c)]. Figure 6(d) shows the  $IQE$  for different V-defect diameters at a V-defect density of  $1.0 \times 10^8 \text{ cm}^{-2}$ . When the diameter increases, the V-defect area increases and the active  $c$ -plane area decreases. Thus, the  $IQE$  decreases with increasing V-defect diameter because of the increased Auger effect, which is consistent with earlier work.<sup>15</sup>

To further to discuss the joint influence of V-defect density and diameter on the  $IQE$ , we consider the ratio of V-defect area to the total chip area. Figure 8(a) shows  $V_{\text{for}}$  as a function of the V-defect area ratio, where points on a given V-defect density curve correspond to the different V-defect diameters (50, 100, 220, 280, and 340 nm), which change the V-defect area ratio. At low V-defect area ratio,  $V_{\text{for}}$  is affected by both the V-defect area ratio<sup>46</sup> and the V-defect density. This result is attributed to the density being too low, even for large V-defects, so the carriers injected from V-defects need to travel

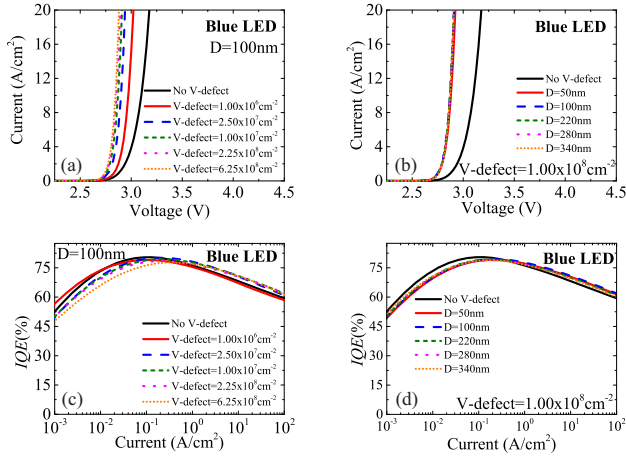


FIG. 6. (a) Voltage versus current for blue LED at different V-defect densities for V-defect diameter  $D = 100$  nm. (b) Voltage versus current for blue LED at different V-defect diameters and a V-defect density of  $1 \times 10^8$   $\text{cm}^{-2}$ . (c)  $IQE$  versus current for blue LED at different V-defect densities and a V-defect diameter of  $D = 100$  nm. (d)  $IQE$  versus current for blue LED at different V-defect diameters and a V-defect density of  $1 \times 10^8$   $\text{cm}^{-2}$ .

through a long lateral region to inject into the entire QW. In addition, the natural alloy potential fluctuations in the QW limit the lateral transport distance of electrons and holes. As a result, carriers become crowded near the V-defect at low V-defect density, so the device performance is strongly limited by the lateral transport distance from the V-defect within the QW.<sup>18</sup>

This result is again verified by Figs. 7(b)–7(d). The recombination becomes less crowded when the V-defect density increases. Once the V-defect area ratio grows larger,  $V_{\text{for}}$  decreases and then saturates at the expected value near 2.7 V. Another contribution comes from the modified vertical injection due to the presence of V-defects: the fluctuations in the vertical energy barriers induced by the random alloy fluctuations causes some carriers to be directly injected from the  $c$  plane in regions with lower barriers. With V-defects, electrons and holes can flow laterally into all quantum wells.<sup>47</sup> Once carriers flow into QWs, they screen the polarization-related electric fields so that vertical current injection directly into  $c$ -plane QWs increases at lower bias voltage compared with the case without V-defects.

The diameter and density of V-defects also affect the efficiency of the blue LED. Since the optimized performance is decided by wall plug efficiency ( $WPE$ ), we estimate the  $WPE$  by assuming a 90% light extraction efficiency (LEE), typical of LEDs grown on patterned sapphire substrates (PSS). We simulated how the  $WPE$  at a fixed 20  $\text{A}/\text{cm}^2$  current density depends on the V-defect area ratio, which corresponds to different diameters and densities of V-defects. The results are shown in Fig. 8(b). Interestingly, the low V-defect density of  $1.0 \times 10^6$  and  $2.5 \times 10^7$   $\text{cm}^{-2}$  have a much lower  $WPE$  and  $IQE$  than the others because the current paths from V-defects to the whole chip area are too long so the constant injected

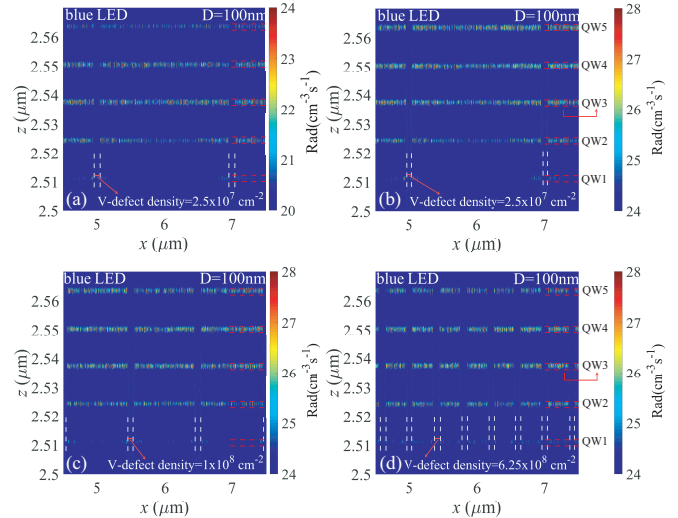


FIG. 7. Distribution of radiative recombination rate for blue LED with  $D = 100$  nm. The plot is at log scale. (a) V-defect density  $2.5 \times 10^7$   $\text{cm}^{-2}$  at current density 0.01  $\text{A}/\text{cm}^2$  (b) V-defect density  $2.5 \times 10^7$   $\text{cm}^{-2}$  at current density 20  $\text{A}/\text{cm}^2$  (c) V-defect density  $1 \times 10^8$   $\text{cm}^{-2}$  at current density 20  $\text{A}/\text{cm}^2$  (d) V-defect density  $6.25 \times 10^8$   $\text{cm}^{-2}$  at current density 20  $\text{A}/\text{cm}^2$ . White dashed lines indicate the location of V-defects on  $x$  axis. The red arrow in panel (b) indicates that the top QW is not injected vertically at low current (bias) and injection occurs through the V-defects. The red dashed lines indicate the QW positions.

current of 20  $\text{A}/\text{cm}^2$  becomes crowded near the V-defect region. They also have a higher  $V_{\text{for}}$ . When the V-defect density exceeds  $1.00 \times 10^8$   $\text{cm}^{-2}$ , which is within the lateral diffusion length, the carriers are easily injected into the whole active region, diminishing crowding and further canceling the quantum-confined Stark effect. This is also seen in Figs. 7(b)–7(d).

This latter effect helps to increase electron-hole overlap and increase the efficiency. However, the  $IQE$  also gradually decreases as the V-defect area ratio further increases because the active volume decreases, and the droop effect starts to dominate at lower current density for larger V-defect area ratio. The conclusion is obvious: it is advantageous (i) to have a high V-defect density so that the V-defect separation is about the lateral carrier transport distance (often referred to as a diffusion length), to inject carriers homogeneously, and (ii) to have small V-defects to minimize nonemitting, unproductive V-defects. The larger V-defects densities also have a smaller  $V_{\text{for}}$ , but the reduction of  $V_{\text{for}}$  saturates as V-defects density becomes larger than  $10^8$   $\text{cm}^{-2}$ . Hence, the  $WPE$  reaches a peak at the V-defect ratio around 5%.

## 2. Performance of green V-defect LED

For the green LED without V-defects,  $V_{\text{for}} = 3.83$  V at 1  $\text{A}/\text{cm}^2$  current density is greater than for the blue LED [Fig. 9(a)].<sup>4,6</sup> If we further remove the barrier doping, as indicated by the black dotted line,  $V_{\text{for}}$  increases. Despite doping the

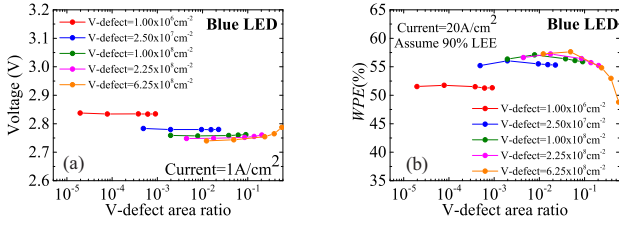


FIG. 8. (a) V-defect region ratio (V-defect area/chip area) versus turn-on voltage for different V-defect densities at a current density of  $1 \text{ A/cm}^2$  for blue LEDs. (b) V-defect region ratio versus  $WPE$  for different V-defect densities at a current density of  $20 \text{ A/cm}^2$  for blue LEDs. The 90% LEE is assumed.

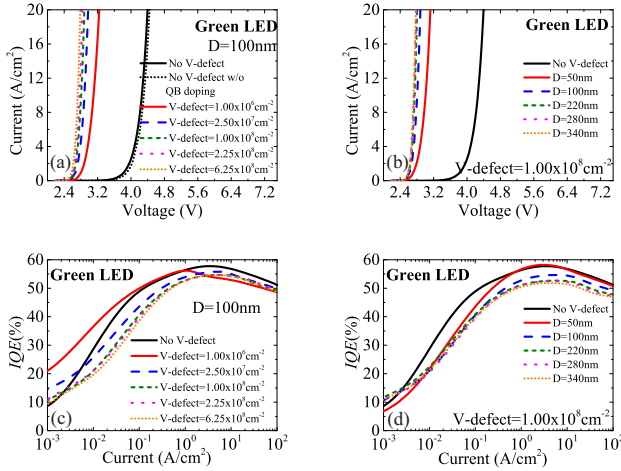


FIG. 9. (a) Voltage versus current for green LED at different V-defect densities and for a V-defect diameter of  $D = 100 \text{ nm}$ . (b) Voltage versus current for green LED at different V-defect diameters and a V-defect density of  $1 \times 10^8 \text{ cm}^{-2}$ . (c)  $IQE$  versus current density for green LED at different V-defect densities and for a V-defect diameter of  $D = 100 \text{ nm}$ . (d)  $IQE$  versus current for green LED at different V-defect diameters and a V-defect density of  $1 \times 10^8 \text{ cm}^{-2}$ .

QB barriers between the MQWs, the polarization barrier induced by the high indium composition is not completely offset. Therefore, V-defects are much more helpful to decrease the turn-on voltage for green LEDs than for blue LEDs. The lowest V-defect density of  $1 \times 10^6 \text{ cm}^{-2}$  decreases the turn-on voltage to  $2.81 \text{ V}$ , as shown in Fig. 9(a).

We also simulated different V-defect densities and find that  $V_{\text{for}}$  decreases as the V-defect density increases. The different diameters of V-defects are also simulated at a density  $1 \times 10^8 \text{ cm}^{-2}$ , as shown in Fig. 9(b). The results are similar to the blue LED shown in Fig. 6(b). The voltage decreases as the diameter increases and then saturates.

We also calculate  $IQE$  versus V-defect density for  $D = 100 \text{ nm}$  [see Fig. 9(c)]. The results show that different V-defect densities produce different performances. Unlike the blue LED where some carriers are injected from the  $c$  plane, in the green LED, most carriers are injected into the planar QWs through the V-defect sidewall, as shown in Figs. 4 and 5. For

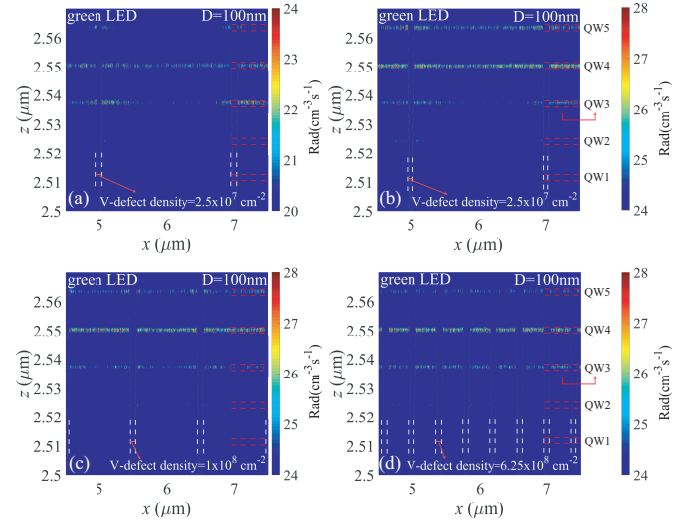


FIG. 10. Distribution of radiative recombination rate for green LED at  $D = 100 \text{ nm}$ . The plot is at log scale. (a) V-defect density  $2.5 \times 10^7 \text{ cm}^{-2}$  at current density  $0.01 \text{ A/cm}^2$ . (b) V-defect density  $2.5 \times 10^7 \text{ cm}^{-2}$  at current density  $20 \text{ A/cm}^2$ . (c) V-defect density  $1 \times 10^8 \text{ cm}^{-2}$  at current density  $20 \text{ A/cm}^2$ . (d) V-defect density  $6.25 \times 10^8 \text{ cm}^{-2}$  at current density  $20 \text{ A/cm}^2$ . Vertical white dashed lines indicate the location of V-defects along the  $x$  axis.

the lower V-defect density, the  $IQE$  peaks slightly higher due to a lower TD density. However, due to greater current crowding, where carriers are crowded in the  $c$ -plane QW near V-defects, the droop effect appears at lower current densities, as shown in Fig. 9(c). When the current density increases, additional carriers flow into the whole active QW region for all V-defect densities. Therefore, the  $IQE$ s reach a similar value for all V-defect densities, as shown in Fig. 9(c).

Figure 9(d) shows the  $IQE$  for different V-defect diameters and for a V-defect density of  $1.0 \times 10^8 \text{ cm}^{-2}$ . For the larger diameters, the V-defect area increases and the active  $c$ -plane area decreases. Thus, the  $IQE$  decreases as the V-defect diameter increases. To further discuss this, we consider how the performance depends on the V-defect area ratio.

Figure 10 shows the recombination distribution for different current densities and different V-defect densities. Unlike for blue LEDs, a strong crowding effect occurs until the V-defect density exceeds  $1 \times 10^8 \text{ cm}^{-2}$ , independently of the current density. This again shows that the V-defect density is the dominant factor for carrier injection. As mentioned in the blue case, if the random alloy fluctuation is not considered, the current crowding effect is not observed, which leads to a much higher  $IQE$  and the delay of droop behavior.

Figure 11(a) shows  $V_{\text{for}}$  versus the V-defect area ratio and for different V-defect densities. Figure 11(a) shows that the turn-on voltage for green LEDs decreases as the V-defect area ratio increases. In addition, green LEDs have a higher indium composition and a higher polarization-related electric field, so only holes flow into the  $c$  plane from V-defects and become crowded at the last QWs, as do electrons [see Fig. 5(b)]. Therefore, the turn-on voltage decreases as the V-defect

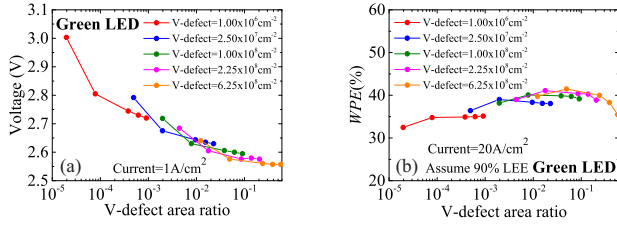


FIG. 11. (a) V-defect region ratio (V-defect area/chip area) versus turn-on voltage for different V-defect densities at a current density 1 A/cm<sup>2</sup> for green LED. (b) V-defect region ratio versus WPE for different V-defect densities at a current density of 20 A/cm<sup>2</sup> for green LED. The 90% LEE is assumed.

area ratio increases. This effect influences WPE of the green LED.

Figure 11(b) shows how the V-defect area ratio affects the WPE at 20 A/cm<sup>2</sup>. Again a 90% LEE is assumed in estimating the WPE. As mentioned,  $V_{\text{for}}$  decreases as the V-defect area ratio increases, which improve the WPE. At the same V-defect area ratio, a greater V-defect density corresponds to a greater IQE. Because carriers are injected into the QW from V-defects and the diffusion length in the fluctuating QWs is short, the IQE depends much more on the V-defect density than on the V-defect diameter. Combining both effects, the WPE reaches a maximum near 5% V-defect area ratio. For the same V-defect area ratio, a high defect density is preferable in green LEDs since they provide a higher IQE for a similar  $V_{\text{for}}$ .

#### IV. CONCLUSION

In contrast with previous analyses of V-defects<sup>15</sup> in LEDs, we computed the influence of both random alloy fluctuations and of V-defect density and size. Random alloy fluctuations help to inject carriers vertically, whereas weak polarization-related electric fields in the inclined sidewalls of V-defects provide an alternative path for lateral carrier injection into the *c*-plane QWs. In blue LEDs, V-defects have only a small impact, mainly reducing  $V_{\text{for}}$  by 0.14 V because carriers are rather efficiently injected vertically. This feature cannot be observed without including both random alloy fluctuation and V-defect. With considering only the V-defect model<sup>15</sup>, carriers can only diffuse into QW through the V-defect where the influence of V-defect density might be overestimated. In green LEDs, the large polarization-related barriers hamper vertical transport, so carriers are preferentially injected from V-defects.  $V_{\text{for}}$  is strongly reduced by about 1.0 V, even at small V-defect density, but the limited lateral diffusion length induces current crowding near V-defects. Therefore, increasing V-defect density increases the peak IQE at large current densities. With the use of an alternative 2D model to 3D models, we could simulate a much larger, realistic area of LEDs and observe the limits of lateral carrier diffusion from V-defects due to random alloy fluctuations, while these features cannot be seen in 3D simulations as the modeled LED size is well below the diffusion length, severely limited by computing re-

sources.

When carriers are injected into the *c*-plane QWs at high bias and current density, they can screen the polarization field and thereby allow more carriers to be injected either through V-defects or vertically through the *c*-plane stack of barriers and wells, thus providing a welcome synergy between V-defects and vertical carrier injection. However, optimization will require further work. Although the increase of V-defect density decreases  $V_{\text{for}}$ , it also reduces the IQE due to a higher possibility to be trapped and recombine nonradiatively in TDs around the center of V-defects. Detailed measurements of these non-radiative parameters are required for precise selection of V-defect density and size.

#### ACKNOWLEDGMENTS

This work was supported by the Ministry of Science and Technology, Taiwan (Grant Nos. MOST 108-2628-E-002-010-MY3, MOST 110-2923-E-002-002, and MOST 111-2923-E-002-009). The work at UCSB was supported by the National Science Foundation (Grant No. DMS-1839077), and by grants from the Simons Foundation (Grant Nos. 601952 to J.S. and 601954 to C.W.). This work was also supported by the TECCLON project, grant ANR-20-CE05-0037-01 of the French Agence Nationale de la Recherche (ANR). Additional support for JSS was provided by the U.S. Department of Energy (Award No. DE-EE0009691). The data used in this paper can be requested by contacting the corresponding author. The modeling tool was developed by the NTU laboratory, and more detailed information can be found on our website (<http://yrwu-wk.ee.ntu.edu.tw/>).

- <sup>1</sup>C. Weisbuch, "On the search for efficient solid state light emitters: Past, present, future," *ECS Journal of Solid State Science and Technology* **9**, 016022 (2019).
- <sup>2</sup>M. Auf der Maur, A. Pecchia, G. Penazzi, W. Rodrigues, and A. Di Carlo, "Efficiency drop in green InGa<sub>N</sub>/Ga<sub>N</sub> light emitting diodes: The role of random alloy fluctuations," *Phys. Rev. Lett.* **116**, 027401 (2016).
- <sup>3</sup>M. Auf der Maur, D. Baretin, A. Pecchia, F. Sacconi, and A. Di Carlo, "Effect of alloy fluctuations in InGa<sub>N</sub>/Ga<sub>N</sub> quantum wells on optical emission strength," in *Numerical Simulation of Optoelectronic Devices, 2014* (2014) pp. 11–12.
- <sup>4</sup>C. Lynsky, A. I. Alhassan, G. Lheureux, B. Bonef, S. P. DenBaars, S. Nakamura, Y.-R. Wu, C. Weisbuch, and J. S. Speck, "Barriers to carrier transport in multiple quantum well nitride-based *c*-plane green light emitting diodes," *Physical Review Materials* **4**, 054604 (2020).
- <sup>5</sup>A. H. Mukund, *InGa<sub>N</sub>/Ga<sub>N</sub> Multiple Quantum Well Light-Emitting Diodes grown on Polar, Semi-polar and Non-Polar Orientations* (North Carolina State University, 2014).
- <sup>6</sup>G. Lheureux, C. Lynsky, Y.-R. Wu, J. S. Speck, and C. Weisbuch, "A 3D simulation comparison of carrier transport in green and blue *c*-plane multiple quantum well nitride light emitting diodes," *Journal of Applied Physics* **128**, 235703 (2020).
- <sup>7</sup>K. Qwah, M. Monavarian, G. Lheureux, J. Wang, Y.-R. Wu, and J. Speck, "Theoretical and experimental investigations of vertical hole transport through unipolar AlGa<sub>N</sub> structures: impacts of random alloy disorder," *Applied Physics Letters* **117**, 022107 (2020).
- <sup>8</sup>T.-J. Yang, R. Shivaraman, J. S. Speck, and Y.-R. Wu, "The influence of random indium alloy fluctuations in indium gallium nitride quantum wells on the device behavior," *Journal of Applied Physics* **116**, 113104 (2014).
- <sup>9</sup>Y.-R. Wu, R. Shivaraman, K.-C. Wang, and J. S. Speck, "Analyzing the physical properties of InGa<sub>N</sub> multiple quantum well light emitting diodes from nano scale structure," *Applied Physics Letters* **101**, 083505 (2012).

- <sup>10</sup>H.-H. Chen, J. S. Speck, C. Weisbuch, and Y.-R. Wu, "Three dimensional simulation on the transport and quantum efficiency of UVC-LEDs with random alloy fluctuations," *Applied Physics Letters* **113**, 153504 (2018).
- <sup>11</sup>M. A. der Maur, A. Pecchia, and A. Di Carlo, "Influence of random alloy fluctuations in InGaN/GaN quantum wells on LED efficiency," in *2015 IEEE 1st International Forum on Research and Technologies for Society and Industry Leveraging a better tomorrow (RTSI)* (IEEE, 2015) pp. 153–156.
- <sup>12</sup>S. Lester, F. A. Ponce, M. G. Craford, and D. A. Steigerwald, "High dislocation densities in high efficiency GaN-based light-emitting diodes," *Applied Physics Letters* **66**, 1249–1251 (1995).
- <sup>13</sup>V. Voronenkov, N. Bochkareva, R. Gorbunov, P. Latyshev, Y. Lelikov, Y. Rebane, A. Tsyuk, A. Zubrilov, and Y. Shreter, "Nature of V-shaped defects in GaN," *Japanese Journal of Applied Physics* **52**, 08JE14 (2013).
- <sup>14</sup>H. Yoshida, T. Hikosaka, H. Nago, and S. Nunoue, "Impact of dislocations and defects on the relaxation behavior of InGaN/GaN multiple quantum wells grown on Si and sapphire substrates," *physica status solidi (b)* **252**, 917–922 (2015).
- <sup>15</sup>C.-K. Li, C.-K. Wu, C.-C. Hsu, L.-S. Lu, H. Li, T.-C. Lu, and Y.-R. Wu, "3d numerical modeling of the carrier transport and radiative efficiency for InGaN/GaN light emitting diodes with v-shaped pits," *AIP Advances* **6**, 055208 (2016).
- <sup>16</sup>Y.-H. Cho, J.-Y. Kim, J. Kim, M.-B. Shim, S. Hwang, S.-H. Park, Y.-S. Park, and S. Kim, "Quantum efficiency affected by localized carrier distribution near the V-defect in GaN based quantum well," *Applied Physics Letters* **103**, 261101 (2013).
- <sup>17</sup>Z. Quan, J. Liu, F. Fang, G. Wang, and F. Jiang, "Effect of V-shaped Pit area ratio on quantum efficiency of blue InGaN/GaN multiple-quantum well light-emitting diodes," *Optical and Quantum Electronics* **48**, 195 (2016).
- <sup>18</sup>H.-T. Shen, C. Weisbuch, J. S. Speck, and Y.-R. Wu, "Three-Dimensional Modeling of Minority-Carrier Lateral Diffusion Length Including Random Alloy Fluctuations in (In, Ga) N and (Al, Ga) N Single Quantum Wells," *Physical Review Applied* **16**, 024054 (2021).
- <sup>19</sup>S. Zhou and X. Liu, "Effect of V-pits embedded InGaN/GaN superlattices on optical and electrical properties of GaN-based green light-emitting diodes," *physica status solidi (a)* **214**, 1600782 (2017).
- <sup>20</sup>X. Wu, C. Elsass, A. Abare, M. Mack, S. Keller, P. Petroff, S. DenBaars, J. Speck, and S. Rosner, "Structural origin of V-defects and correlation with localized excitonic centers in InGaN/GaN multiple quantum wells," *Applied Physics Letters* **72**, 692–694 (1998).
- <sup>21</sup>Y.-L. Hu, R. M. Farrell, C. J. Neufeld, M. Iza, S. C. Cruz, N. Pfaff, D. Simeonov, S. Keller, S. Nakamura, S. P. DenBaars, U. K. Mishra, and J. S. Speck, "Effect of quantum well cap layer thickness on the microstructure and performance of InGaN/GaN solar cells," *Applied Physics Letters* **100**, 161101 (2012).
- <sup>22</sup>A. Romanov, T. Baker, S. Nakamura, J. Speck, and E. U. Group, "Strain-induced polarization in wurtzite III-nitride semipolar layers," *Journal of Applied Physics* **100**, 023522 (2006).
- <sup>23</sup>F. Jiang, J. Zhang, L. Xu, J. Ding, G. Wang, X. Wu, X. Wang, C. Mo, Z. Quan, X. Guo, C. Zheng, S. Pan, and J. Liu, "Efficient InGaN-based yellow-light-emitting diodes," *Photonics Research* **7**, 144–148 (2019).
- <sup>24</sup>C. Lynsky, R. C. White, Y. C. Chow, W. Y. Ho, S. Nakamura, S. P. DenBaars, and J. S. Speck, "Role of V-defect density on the performance of III-nitride green LEDs on sapphire substrates," *Journal of Crystal Growth* **560**, 126048 (2021).
- <sup>25</sup>S.-H. Han, D.-Y. Lee, H.-W. Shim, J. Wook Lee, D.-J. Kim, S. Yoon, Y. Sun Kim, and S.-T. Kim, "Improvement of efficiency and electrical properties using intentionally formed V-shaped pits in InGaN/GaN multiple quantum well light-emitting diodes," *Applied Physics Letters* **102**, 251123 (2013).
- <sup>26</sup>C. Ren, B. Rouet-Leduc, J. Griffiths, E. Bohacek, M. Wallace, P. Edwards, M. Hopkins, D. Allsopp, M. Kappers, R. Martin, and R. Oliver, "Analysis of defect-related inhomogeneous electroluminescence in InGaN/GaN QW LEDs," *Superlattices and Microstructures* **99**, 118–124 (2016).
- <sup>27</sup>R. Bouveyron, M. Mrad, and M. Charles, "V-pit pinning at the interface of high and low-temperature gallium nitride growth," *Japanese Journal of Applied Physics* **58**, SC1035 (2019).
- <sup>28</sup>A. Di Vito, A. Pecchia, A. Di Carlo, and M. Auf der Maur, "Simulating random alloy effects in III-nitride light emitting diodes," *Journal of Applied Physics* **128**, 041102 (2020).
- <sup>29</sup>M. Filoche, M. Piccardo, Y.-R. Wu, C.-K. Li, C. Weisbuch, and S. Mayboroda, "Localization landscape theory of disorder in semiconductors. I. Theory and modeling," *Physical Review B* **95**, 144204 (2017).
- <sup>30</sup>M. Piccardo, C.-K. Li, Y.-R. Wu, J. S. Speck, B. Bonafant, R. M. Farrell, M. Filoche, L. Martinelli, J. Peretti, and C. Weisbuch, "Localization landscape theory of disorder in semiconductors. ii. Urbach tails of disordered quantum well layers," *Phys. Rev. B* **95**, 144205 (2017).
- <sup>31</sup>C.-K. Li, M. Piccardo, L.-S. Lu, S. Mayboroda, L. Martinelli, J. Peretti, J. S. Speck, C. Weisbuch, M. Filoche, and Y.-R. Wu, "Localization landscape theory of disorder in semiconductors. III. Application to carrier transport and recombination in light emitting diodes," *Physical Review B* **95**, 144206 (2017).
- <sup>32</sup>D. N. Arnold, G. David, D. Jerison, S. Mayboroda, and M. Filoche, "Effective Confining Potential of Quantum States in Disordered Media," *Phys. Rev. Lett.* **116**, 056602 (2016).
- <sup>33</sup>M. Filoche and S. Mayboroda, "Universal mechanism for Anderson and weak localization," *Proceedings of the National Academy of Sciences* **109**, 14761–14766 (2012).
- <sup>34</sup>E. Kioupakis, P. Rinke, K. T. Delaney, and C. G. Van de Walle, "Indirect Auger recombination as a cause of efficiency droop in nitride light-emitting diodes," *Applied Physics Letters* **98**, 161107 (2011).
- <sup>35</sup>L. C. Le, D. G. Zhao, D. S. Jiang, L. Li, L. L. Wu, P. Chen, Z. S. Liu, Z. C. Li, Y. M. Fan, J. J. Zhu, H. Wang, S. M. Zhang, and H. Yang, "Carriers capturing of V-defect and its effect on leakage current and electroluminescence in InGaN-based light-emitting diodes," *Applied Physics Letters* **101**, 252110 (2012).
- <sup>36</sup>X. Wu, J. Liu, Z. Quan, C. Xiong, C. Zheng, J. Zhang, Q. Mao, and F. Jiang, "Electroluminescence from the sidewall quantum wells in the V-shaped pits of InGaN light emitting diodes," *Applied Physics Letters* **104**, 221101 (2014).
- <sup>37</sup>M. Shiojiri, C. Chuo, J. Hsu, J. Yang, and H. Saijo, "Structure and formation mechanism of V defects in multiple In Ga N / Ga N quantum well layers," *Journal of applied physics* **99**, 073505 (2006).
- <sup>38</sup>C.-Y. Chang, H. Li, Y.-T. Shih, and T.-C. Lu, "Manipulation of nanoscale V-pits to optimize internal quantum efficiency of InGaN multiple quantum wells," *Applied Physics Letters* **106**, 091104 (2015).
- <sup>39</sup>S. Tomiya, Y. Kanitani, S. Tanaka, T. Ohkubo, and K. Hono, "Atomic scale characterization of GaInN/GaN multiple quantum wells in V-shaped pits," *Applied Physics Letters* **98**, 181904 (2011).
- <sup>40</sup>S. Zhou, X. Liu, H. Yan, Y. Gao, H. Xu, J. Zhao, Z. Quan, C. Gui, and S. Liu, "The effect of nanometre-scale V-pits on electronic and optical properties and efficiency droop of GaN-based green light-emitting diodes," *Scientific reports* **8**, 1–12 (2018).
- <sup>41</sup>K. Kumakura, T. Makimoto, N. Kobayashi, T. Hashizume, T. Fukui, and H. Hasegawa, "Minority carrier diffusion length in GaN: Dislocation density and doping concentration dependence," *Applied Physics Letters* **86**, 052105 (2005).
- <sup>42</sup>S. Y. Karpov and Y. N. Makarov, "Dislocation effect on light emission efficiency in gallium nitride," *Applied Physics Letters* **81**, 4721–4723 (2002).
- <sup>43</sup>C. A. Robertson, K. S. Qwah, Y.-R. Wu, and J. S. Speck, "Modeling dislocation-related leakage currents in GaN p-n diodes," *Journal of Applied Physics* **126**, 245705 (2019), <https://doi.org/10.1063/1.5123394>.
- <sup>44</sup>K. S. Qwah, C. A. Robertson, Y.-R. Wu, and J. Speck, "Modeling dislocation-related reverse bias leakage in GaN p-n diodes," *Semiconductor Science and Technology* (2021), 10.1088/1361-6641/abdfdc.
- <sup>45</sup>H.-Y. Ryu, H.-S. Kim, and J.-I. Shim, "Rate equation analysis of efficiency droop in InGaN light-emitting diodes," *Applied Physics Letters* **95**, 081114 (2009).
- <sup>46</sup>C. Wang, Y. Chiou, and H. Chang, "Investigating the Efficiency Droop of Nitride-Based Blue LEDs with Different Quantum Barrier Growth Rates," *Crystals* **9**, 677 (2019).
- <sup>47</sup>Y. Li, W. Tang, Y. Zhang, M. Guo, Q. Li, X. Su, A. Li, and F. Yun, "Nanoscale characterization of V-defect in InGaN/GaN QWs LEDs using near-field scanning optical microscopy," *Nanomaterials* **9**, 633 (2019).